Electronic Supplementary Information

Unveiling poly*a*morphism and poly*a*morphic interconversions in pharmaceuticals: the peculiar case of hydrochlorothiazide

Inês C. B. Martins*[a], Anders S. Larsen[a], Anders Ø. Madsen[a], Olivia Aalling Frederiksen[b], Alexandra Correia,[c] Kirsten M. Ø. Jensen[b], Henrik S. Jeppesen,[d] Thomas Rades*[a]

[a]Department of Pharmacy, University of Copenhagen, Universitetsparken 2, 2100 Copenhagen, Denmark; [b]Department of Chemistry, University of Copenhagen, Universitetsparken 5, 2100 Copenhagen, Denmark; [c]Division of Pharmaceutical Chemistry and Technology, University of Helsinki, Viikinkaari 5, 00790 Helsinki, Finland; [d]Deutsches Elektronen-Synchrotron (DESY), Notkestrasse 85, D-22607 Hamburg, Germany

Table of content

Materials and methods

Hydrochlorothiazide (HCT) form I (purity > 99%) was purchased from Sigma Aldrich. For the preparation of amorphous HCT, three different methods were used: i) spray-drying (SD) – 2 g of HCT were dissolved in 600 mL of ethanol and SD was performed using a Büchi-B290 Mini Spray Dryer (Büchi Labortechnik AG, Flawil, Switzerland) with the following parameters: inlet temperature 80 °C, outlet temperature 47°C, pumping setting 30% and aspirator setting 100%. The collected powder was immediately analyzed by PXRD and mDSC; ii) quench-cooling (QC) – 400 mg of HCT was heated until its melting temperature (276 °C) and cooled to room temperature. Ice and liquid nitrogen were also used in additional QC experiments to evaluate the influence of the cooling rate in the process; iii) ball milling (BM) – 150 mg of HCT were placed in a stainless steel milling jar of 5 mL together with a stainless steel milling ball of 9 mm diameter. The BM experiments were performed using a horizontal ball mill (Mixer mill MM400, Retsch GmbH & Co., Hann, Germany) with a 30 Hz frequency at different times (5 min, 10 min, 15 min, 30 min, 45 min, 60 min, 75 min, 90 min, 105 min and 120 min). For each milling time, fresh samples were used. A total of 10 independent experiments were performed.

Thermogravimetric analysis (TGA)

HCT amorphous samples were measured using a TA-Discovery TGA (TA instruments, New Castle, USA). Approximately 5-7 mg of sample was placed into platinum pans and heated from room temperature to 300 °C at a heating rate of 5 °C/min. Moisture content (water and ethanol) was calculated as weight loss between room temperature and 140 °C. The resulting weight-temperature thermograms are presented in Fig. 2b, S1 and S2.

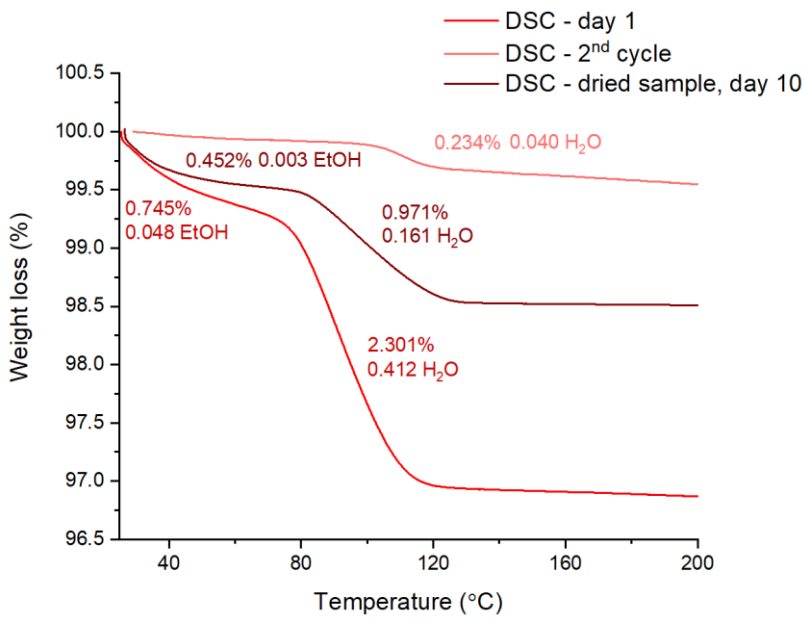

Fig. S1 TGA of HCT poly*a*morphs prepared by SD after 1 and 10 days of drying in a desiccator containing phosphorous pentoxide and after implementing the second heating cycle.

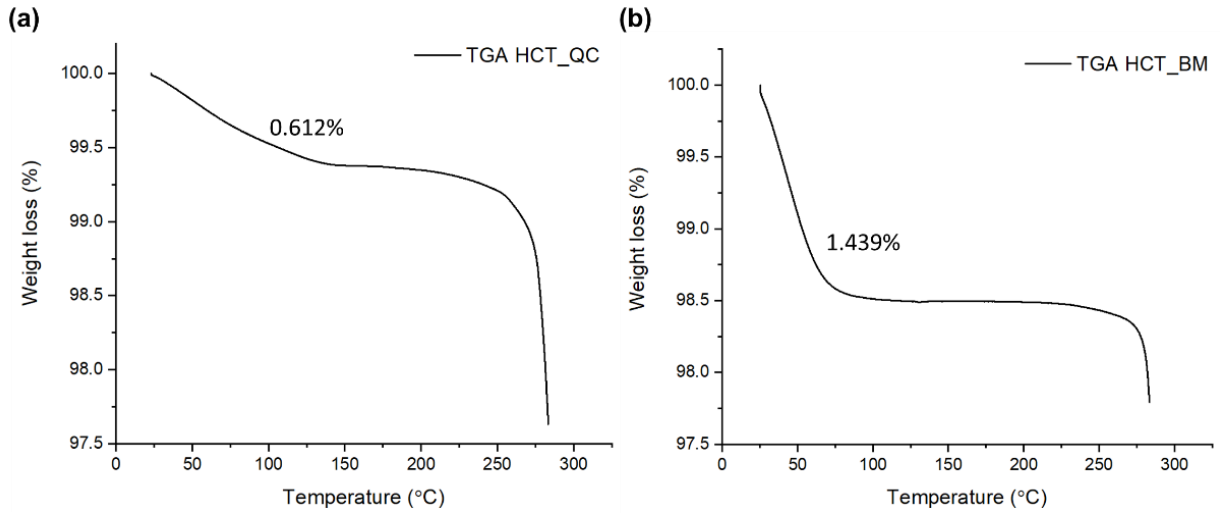

Fig. S2 TGA of HCT poly*a*morphs II and III prepared by QC and BM, respectively, without drying.

Karl Fischer titration

HCT samples were inserted in a vessel under control environment (nitrogen atmosphere in a glovebox). Methanol (5 – 10 mL) was added until all samples were dissolved. Table S1 contains all information about the amount of sample injected and the water content measured using a C10S Coulometric KF Titrator (Mettler Toledo, USA) equipment.

Table S1 Karl Fischer titration results containing the amount of sample injected and the detected water content (%). All samples were kept in a desiccator containing phosphorous pentoxide for two weeks before Karl Fischer titration.

	Sample name	Solvent	Solvent Volume		Sample injected		Water Conc. (%)
	Methanol			ml	3.1784	g	0.05
1	HCT-SD	Methanol	6	ml	3.0750	g	0.6
2	HCT-BM	Methanol	9	ml	3.1389	g	0.3
3	HCT-QC	Methanol	5	ml	3.0314	g	0.11
4	HCT-SD-BM	Methanol	10	ml	3.1655	g	0.4
5	HCT-SD-QC	Methanol	7	ml	3.1104	g	0.1
6	HCT-QC-SD	Methanol	5	ml	2.8422	g	0.2
7	HCT-QC-BM	Methanol	6	ml	3.1688	g	0.08
8	HCT-BM-SD	Methanol	7	ml	3.124	g	0.5
9	HCT-BM-QC	Methanol	5	ml	1.7283	g	0.16

Powder X-ray diffraction (PXRD)

PXRD patterns were collected with a X'Pert PRO X-ray diffractometer (PANalytical, Almelo, The Netherlands) using Cu Kα radiation (λ = 1.54187 Å) at ambient temperature. All scanning was performed at the voltage of 45 kV and current of 40 mA, from 5-35° 2θ, with a scan speed of 0.067 2θ/s and a step size of 0.026. Data was collected and analyzed using the software X'Pert Data Collector 2.2i (PANalytical B.V., Almelo, The Netherlands).

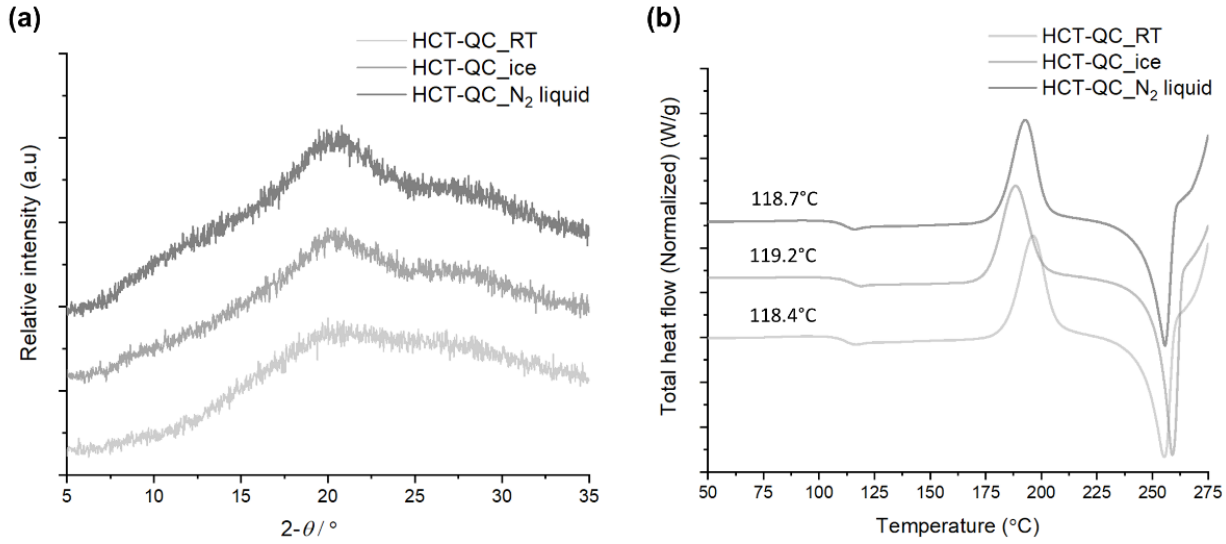

Fig. S3 PXRD (a) and DSC (b) data of HCT poly*a*morph II obtained at different cooling rates.

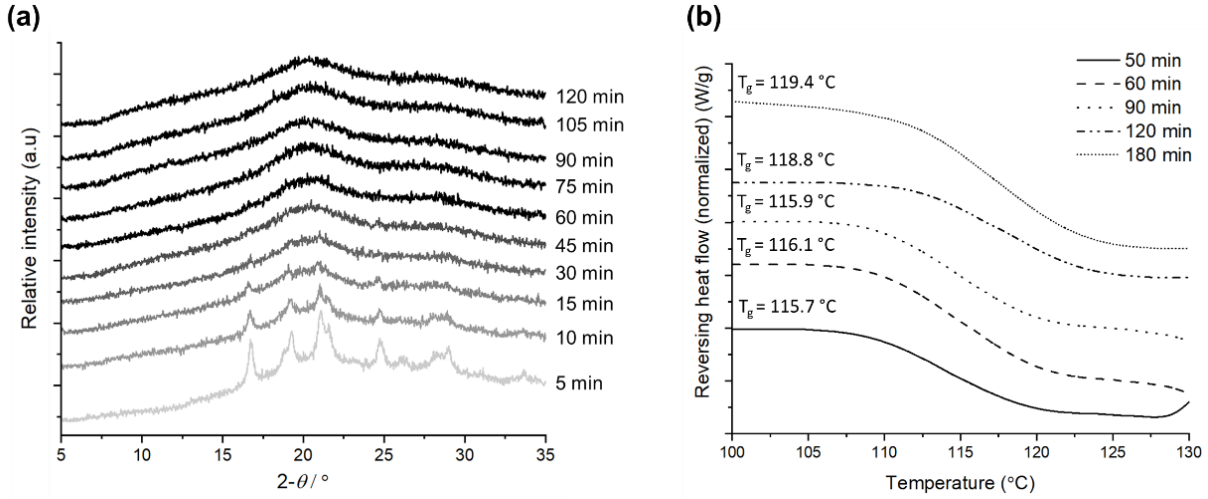

Fig. S4 PXRD (a) and DSC (b) data of HCT poly*a*morph III obtained at different milling times.

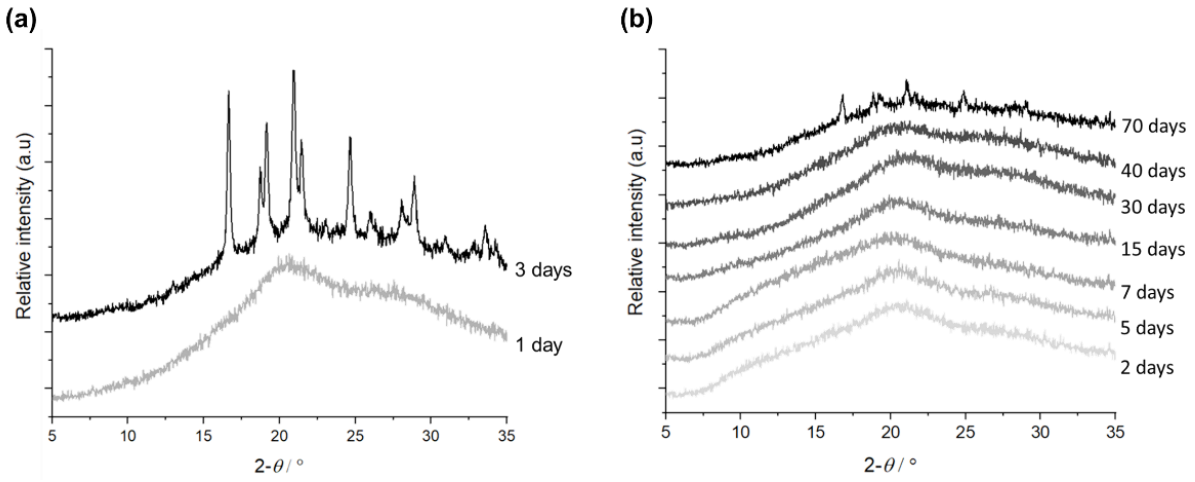

Fig. S5 PXRD of HCT poly*a*morph I after storage under normal room temperature and humidity conditions (a) and in phosphorous pentoxide with activated silica (b).

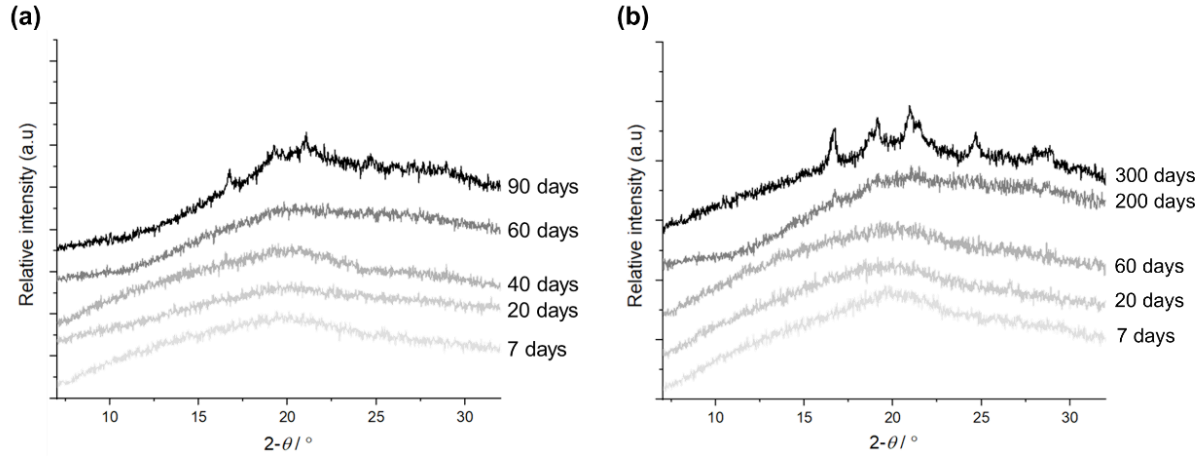

Fig. S6 PXRD of HCT poly*a*morph II after storage under normal room temperature and humidity conditions (a) and in phosphorous pentoxide with activated silica (b).

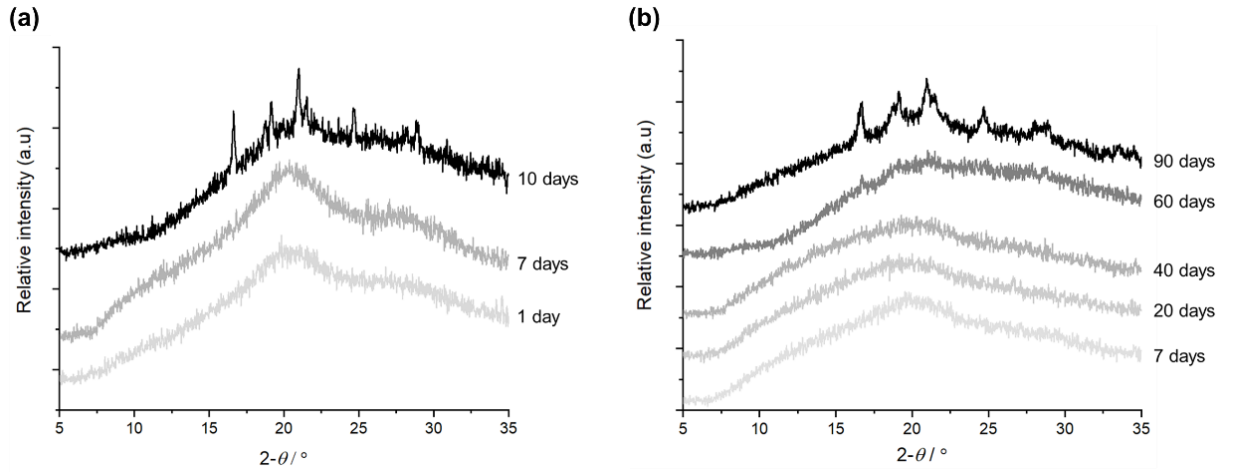

Fig. S7 PXRD of HCT poly*a*morph III after storage under normal room temperature and humidity conditions (a) and in phosphorous pentoxide with activated silica (b).

High performance liquid chromatography (HPLC)

HPLC analysis of crystalline HCT and the respective poly*a*morphs (Fig. S8-S24) was performed with a Finnigan Surveyor Plus HPLC (Thermo Scientific®, USA) instrument equipped with a diode-array detector. A Discovery® C-18 column (150 mm 4 mm; 5 µm particle diameter, end-capped) was used and kept at 25 °C in a thermostatted column compartment. The mobile phase consisted of 95% (V/V) acetonitrile and 5% (V/V) of water. The flow rate was set to 1.2 mL/min and the detection wavelength used was 272 nm. Solutions of 10 µg/mL were prepared by dissolving crystalline HCT and all poly*a*morphs by dissolving HCT in acetonitrile. The injection volume for all samples was 5 µL. The limit of detection (LOD) and the limit of quantification (LOQ) of HCT were calculated using the following equations: LOD = 3N/*m* and LOQ = 10N/*m*; where N is the standard deviation of the peak areas (seven injections) and *m* the slope of the corresponding calibration curve. The LOD and LOQ were 5.7 $\mu g.mL^{-1}$ and 19.2 $\mu g.mL^{-1}$, respectively, for HCT in ethanol, and 1.3 $\mu g.mL^{-1}$ and 4.3 $\mu g.mL^{-1}$ for HCT in water. The calibration curve was as follows: Y = 11.982X, where Y = peak-area ratio (component/internal standard) and X = component concentration ($\mu g.mL^{-1}$). The calibration curve was linear over the concentration range of 0.5-100 $\mu g.mL^{-1}$ with an R=0.99. These values are in accordance with the literature.[1]

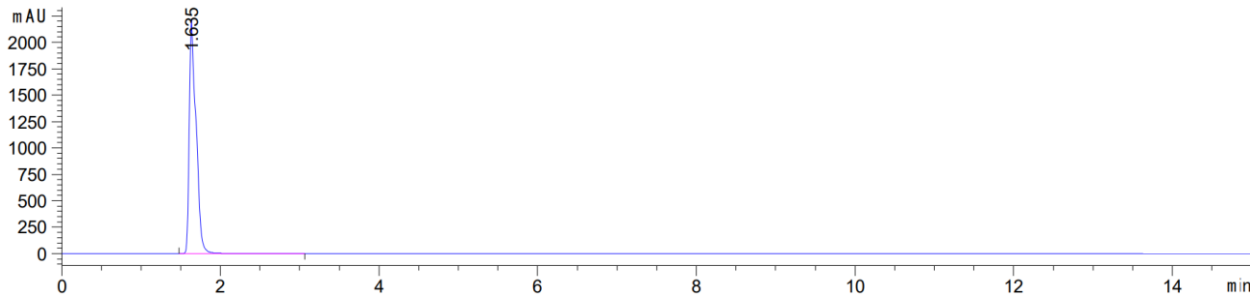

Fig. S8 HPLC curve of crystalline HCT.

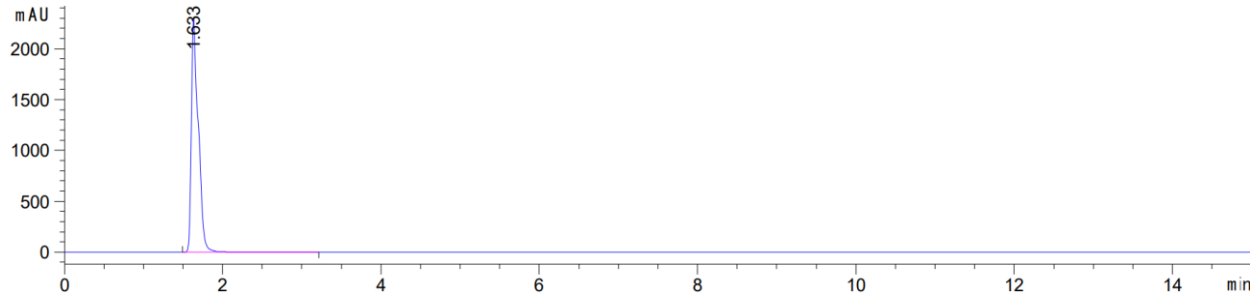

Fig. S9 HPLC curve of amorphous HCT obtained by SD (poly*a*morph I).

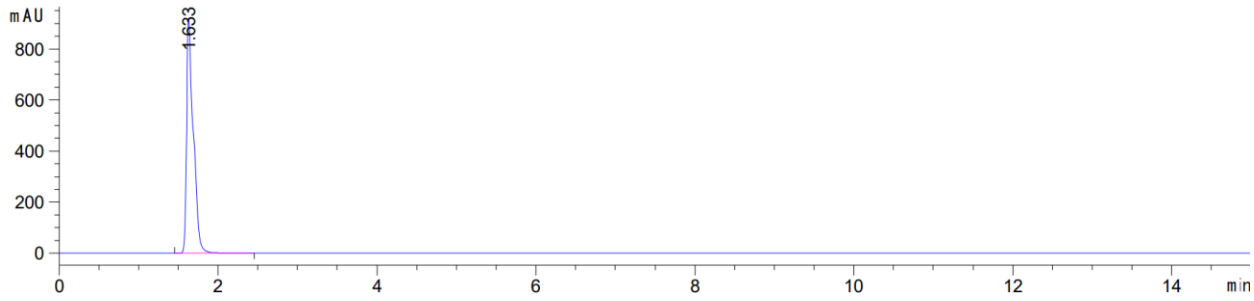

Fig. S10 HPLC curve of amorphous HCT obtained by QC at 275°C (poly*a*morph II).

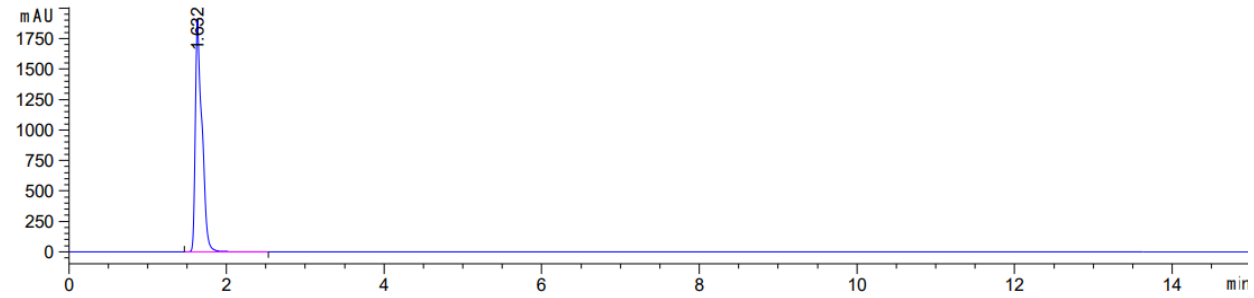

Fig. S11 HPLC curve of amorphous HCT obtained by 1 h of BM (poly*a*morph III).

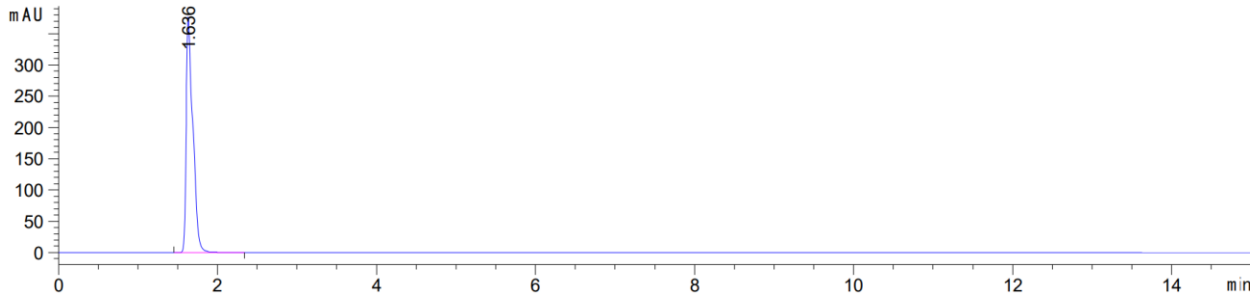

Fig. S12 HPLC curve of amorphous HCT obtained by 1 h of BM after SD (HCT-SD-BM).

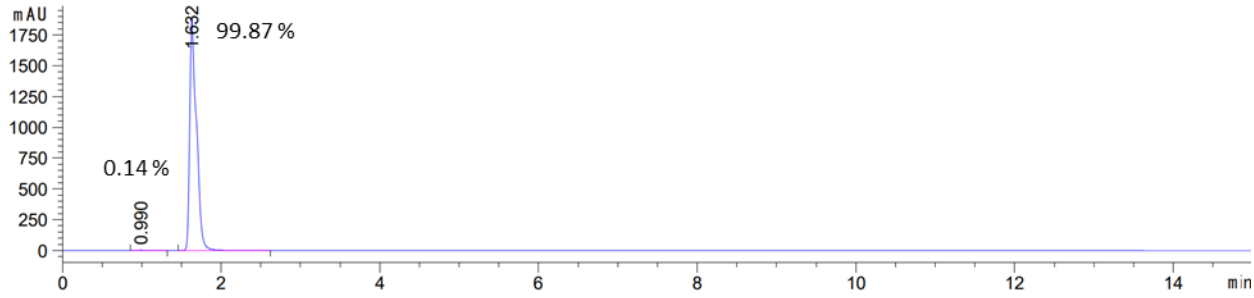

Fig. S13 HPLC curve of amorphous HCT obtained by 2 h of BM after SD (HCT-SD-BM).

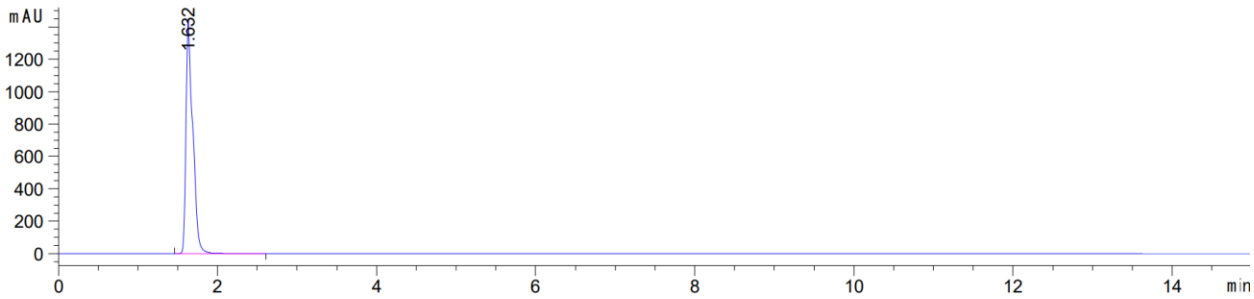

Fig. S14 HPLC curve of amorphous HCT obtained by QC at 275 °C after SD (HCT-SD-QC).

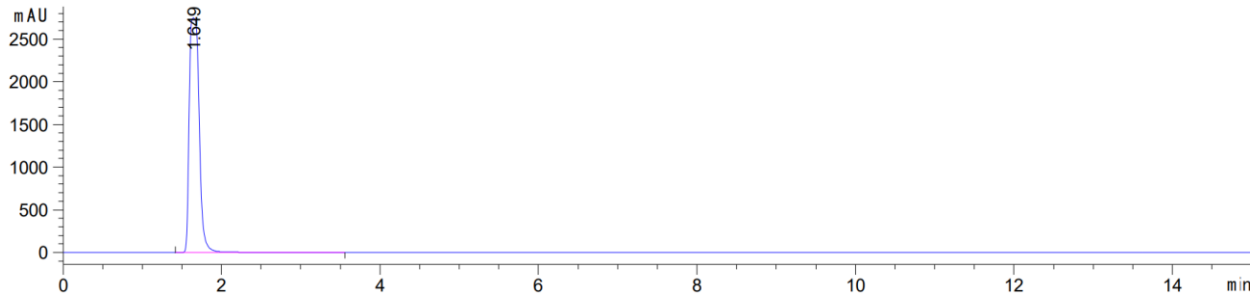

Fig. S15 HPLC curve of amorphous HCT obtained by QC at 280 °C after SD (HCT-SD-QC).

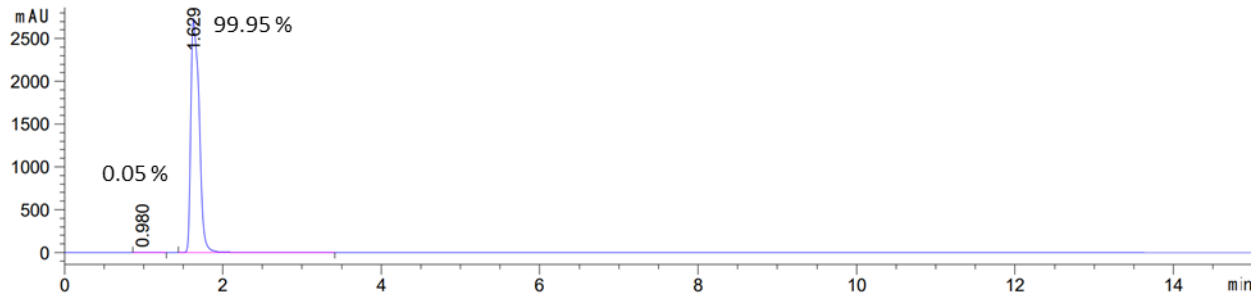

Fig. S16 HPLC curve of amorphous HCT obtained by QC at 283 °C after SD (HCT-SD-QC).

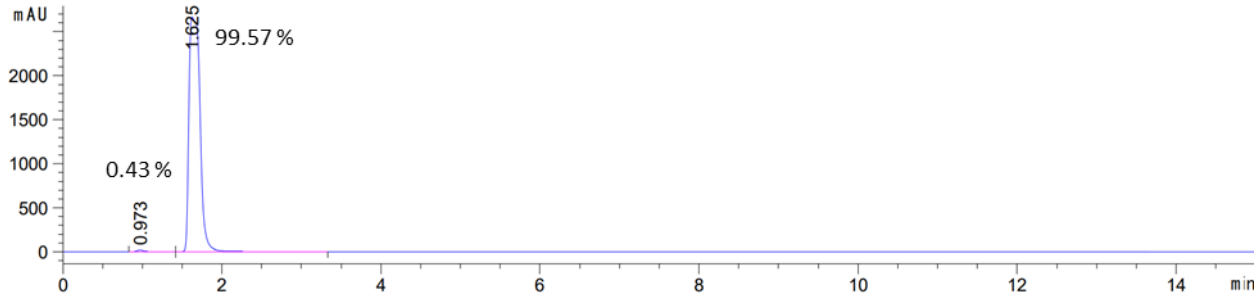

Fig. S17 HPLC curve of amorphous HCT obtained by QC at 290 °C after SD (HCT-SD-QC).

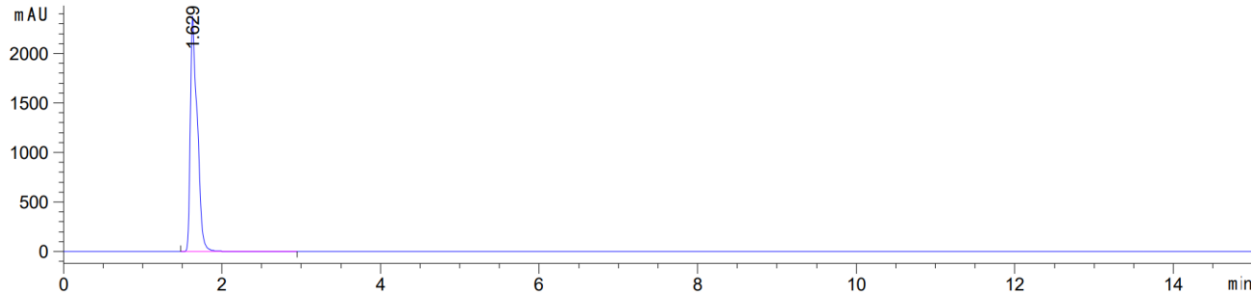

Fig. S18 HPLC curve of amorphous HCT obtained by SD after QC at 275 °C (HCT-QC-SD).

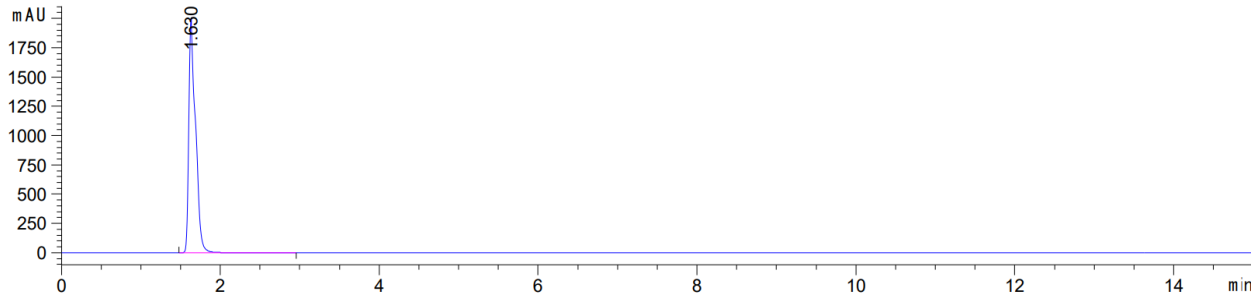

Fig. S19 HPLC curve of amorphous HCT obtained by 1h BM after QC at 275 °C (HCT-QC-BM).

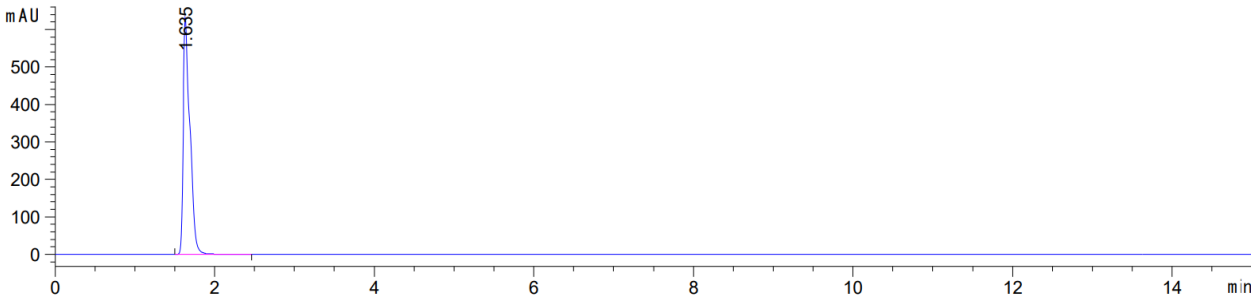

Fig. S20 HPLC curve of amorphous HCT obtained by SD after BM for 1 h (HCT-BM-SD).

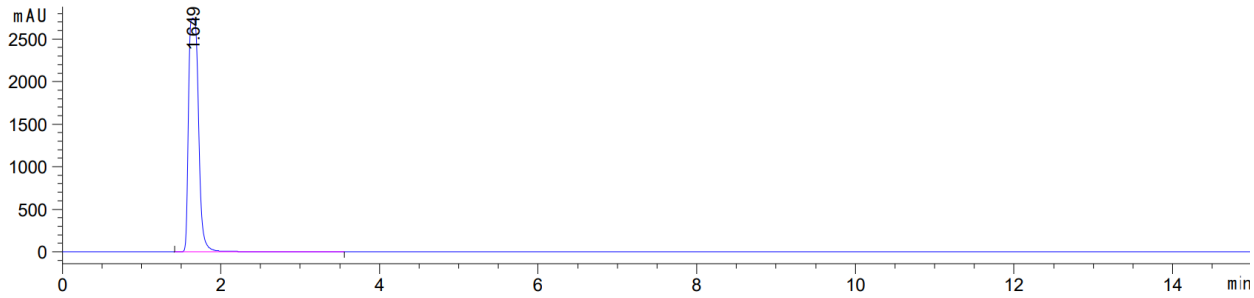

Fig. S21 HPLC curve of amorphous HCT obtained by QC at 275 °C after BM for 1 h (HCT-BM-QC).

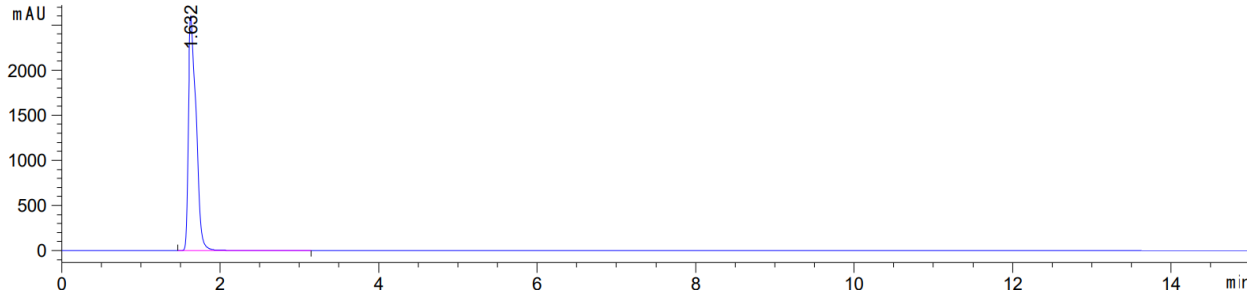

Fig. S22 HPLC curve of amorphous HCT obtained by QC at 280 °C after BM for 1 h (HCT-BM-QC).

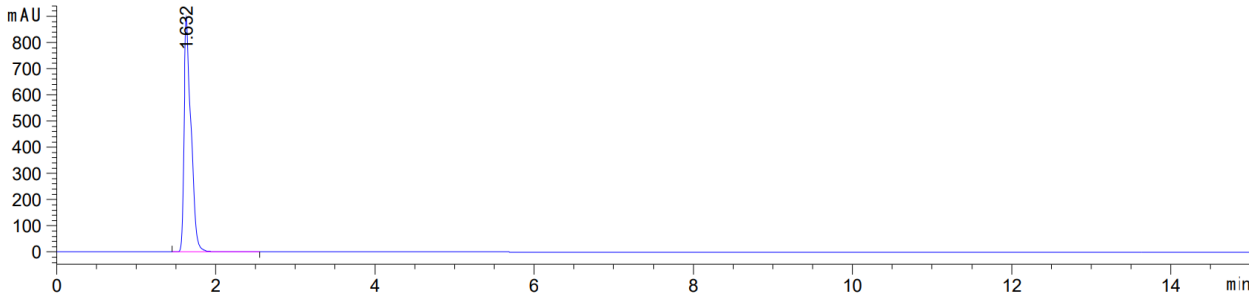

Fig. S23 HPLC curve of amorphous HCT obtained by QC at 283 °C after BM for 1 h (HCT-BM-QC).

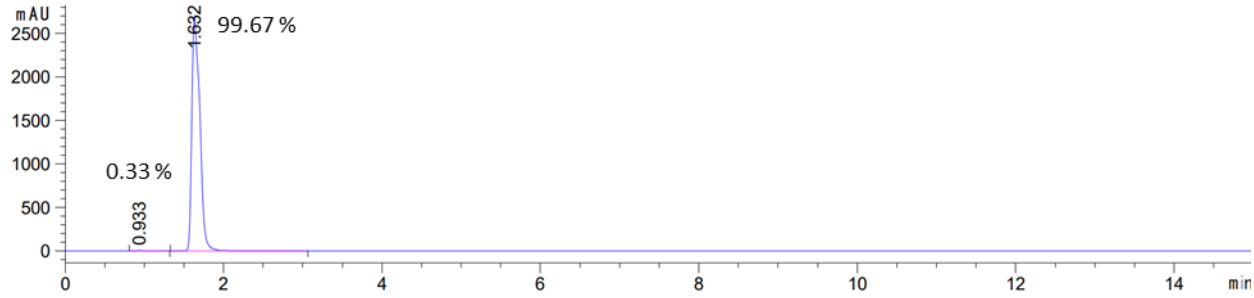

Fig. S24 HPLC curve of amorphous HCT obtained by QC at 290 °C after BM for 1 h (HCT-BM-QC).

Fourier Transform Infrared Spectroscopy (FTIR-ATR)

Three iterative QC experiments were performed for HCT at 275°C using a hot plate. At each QC cycle, the sample was removed from the plate and FTIR-ATR data (Fig. S25) was collected in a Nicolet™ iS50 FTIR Spectrometer and analyzed with OMNIC software.

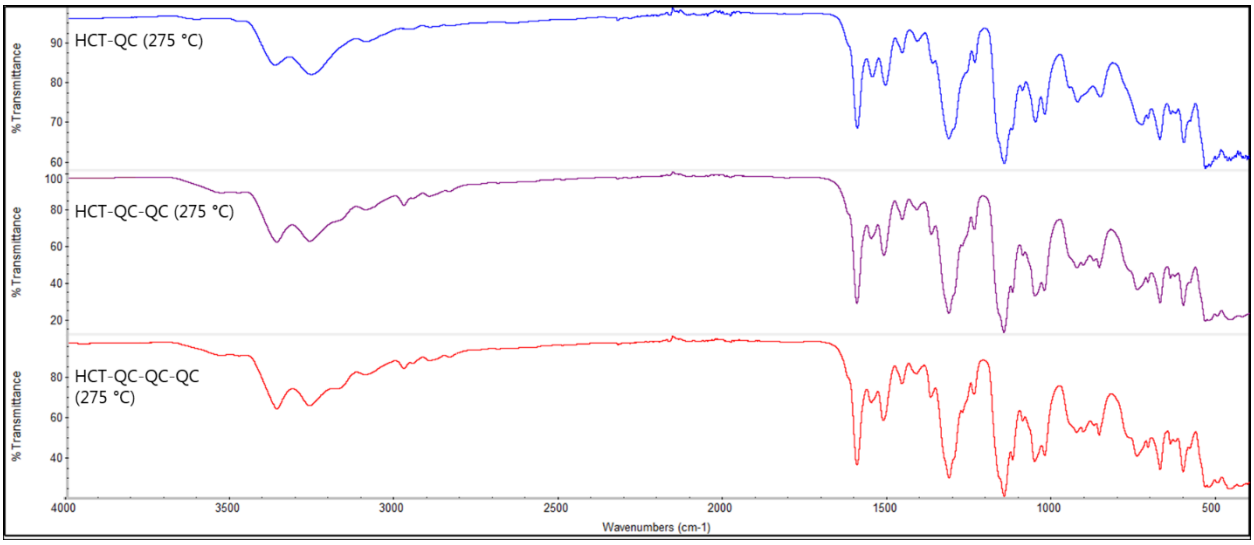

Fig. S25 FTIR-ATR data of HCT after three iterative QC experiments.

Degradation experiments

HCT was QC at 275°C, 280°C and 290°C (degradation). After melting at each temperature, the samples were kept at high temperature for 10 min, 30 min and 2 h before cooling down to room temperature. All samples were analyzed by HPLC and FTIR-ATR (following the procedures described above) and the data is presented in Fig. S26-S35.

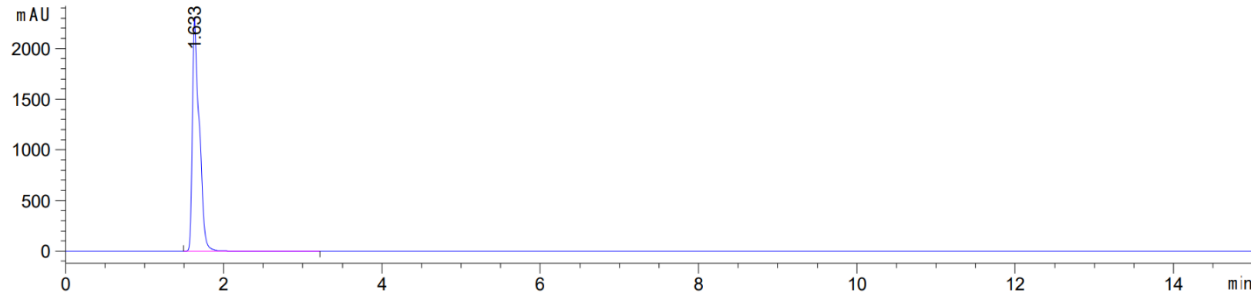

Fig. S26 HPLC curve of amorphous HCT obtained by QC at 275 °C for 10 min.

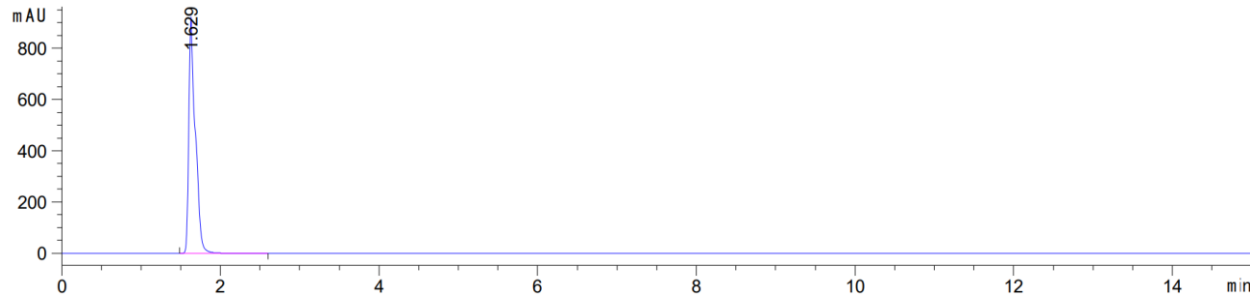

Fig. S27 HPLC curve of amorphous HCT obtained by QC at 275 °C for 30 min.

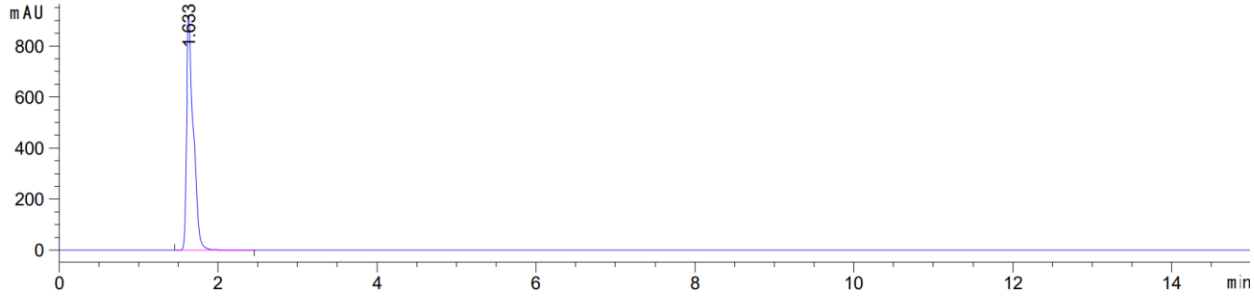

Fig. S28 HPLC curve of amorphous HCT obtained by QC at 275 °C for 2 h.

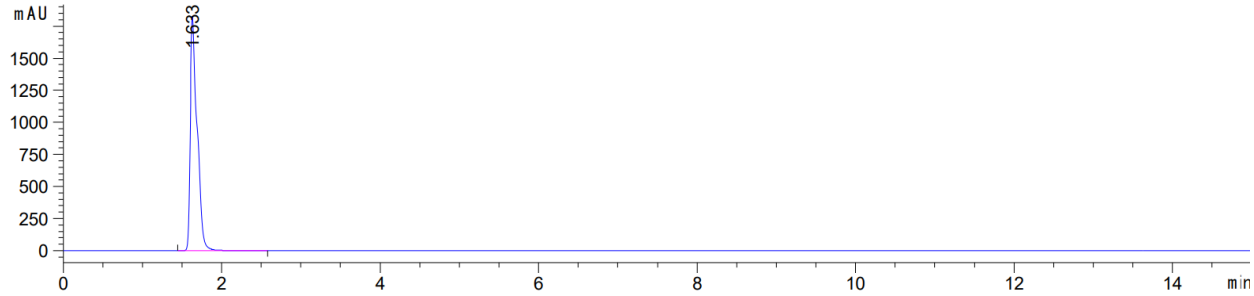

Fig. S29 HPLC curve of amorphous HCT obtained by QC at 280 °C for 10 min.

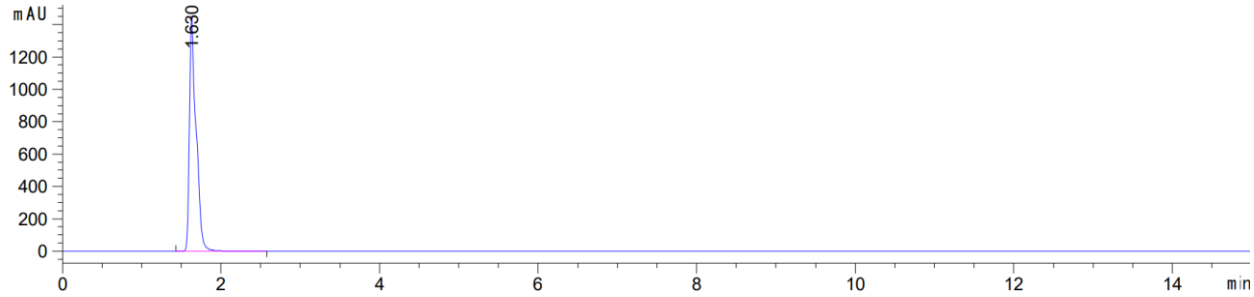

Fig. S30 HPLC curve of amorphous HCT obtained by QC at 280 °C for 30 min.

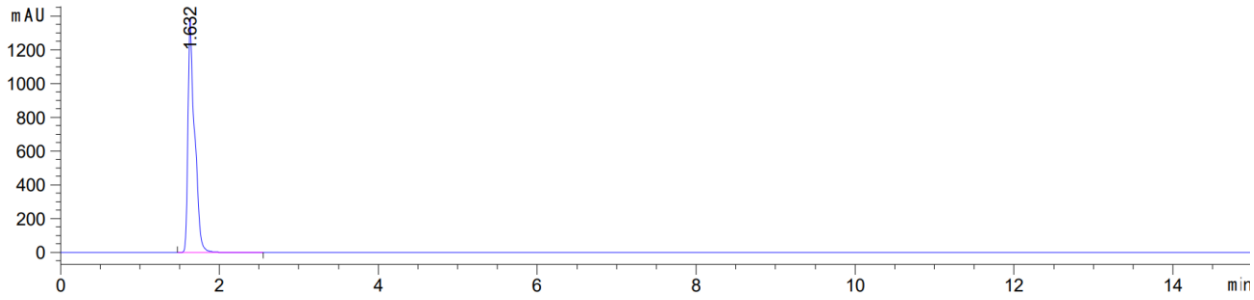

Fig. S31 HPLC curve of amorphous HCT obtained by QC at 280 °C for 2 h.

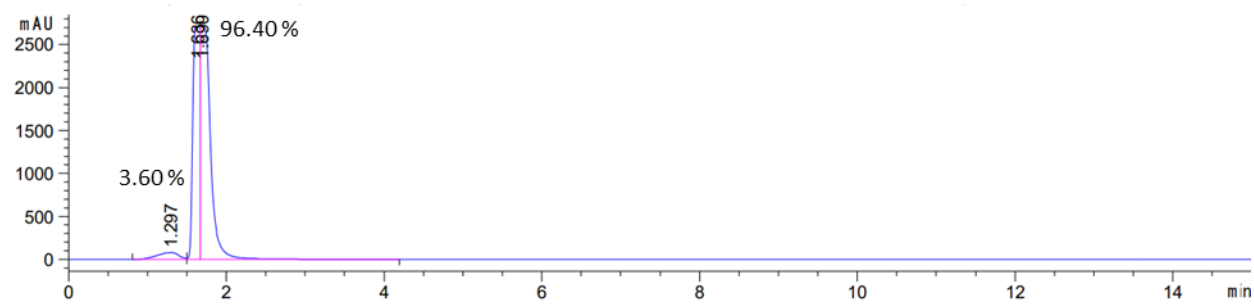

Fig. S32 HPLC curve of amorphous HCT obtained by QC at 290 °C for 10 min.

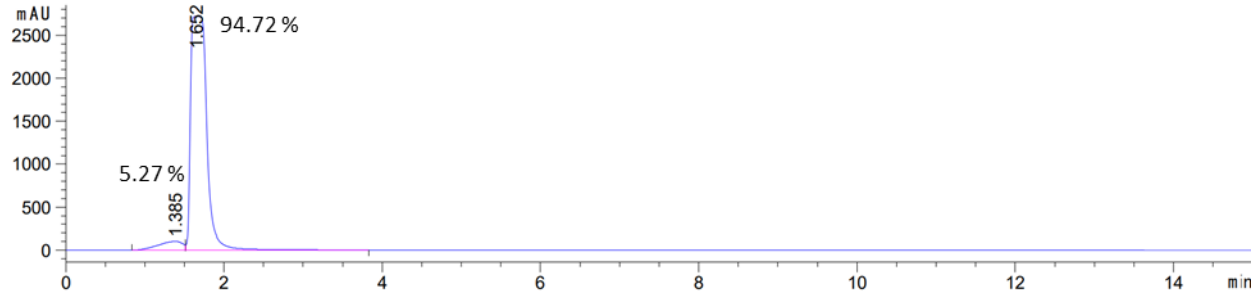

Fig. S33 HPLC curve of amorphous HCT obtained by QC at 290 °C for 30 min.

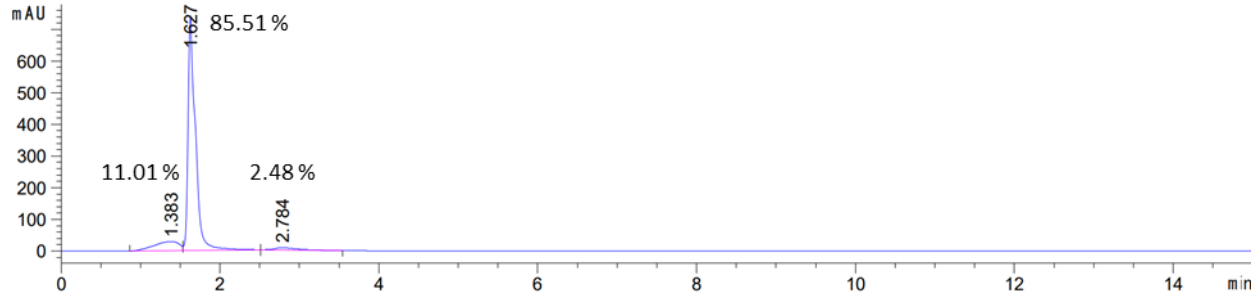

Fig. S34 HPLC curve of amorphous HCT obtained by QC at 290 °C for 2 h.

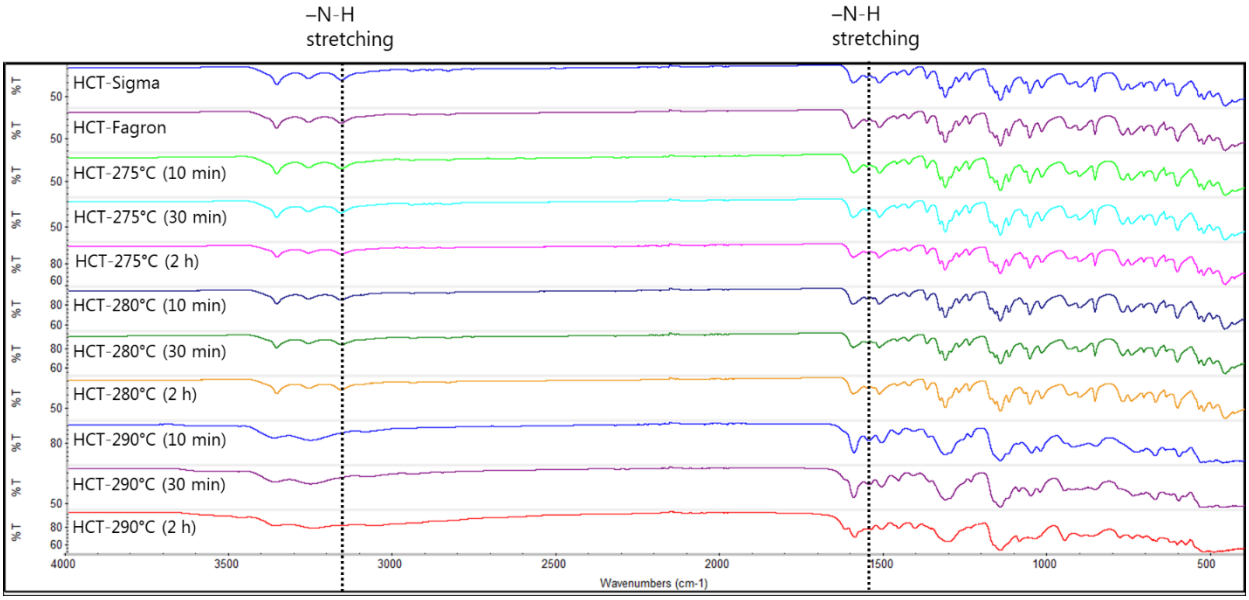

Fig. S35 FTIR-ATR data of HCT after QC at 275°C, 280°C and 290°C and kept at high temperature for different time periods (10 min, 30 min and 2h) .

Modulated differential scanning calorimetry (*m*DSC)

*m*DSC measurements were conducted with Discovery DSC (TA Instruments, New Castle, USA). Samples were heated in modulated temperature mode from -20 to 180 °C with an applied heating rate of 2 °C/min, modulation amplitude of 0.2120 °C, and a period of 40 s. The nitrogen gas flow used was 50 mL/min. Data was analyzed by Trios software (TA Instruments-Waters LLC, New Castle, USA). The T_g values were calculated as the onset of the glass transition events.

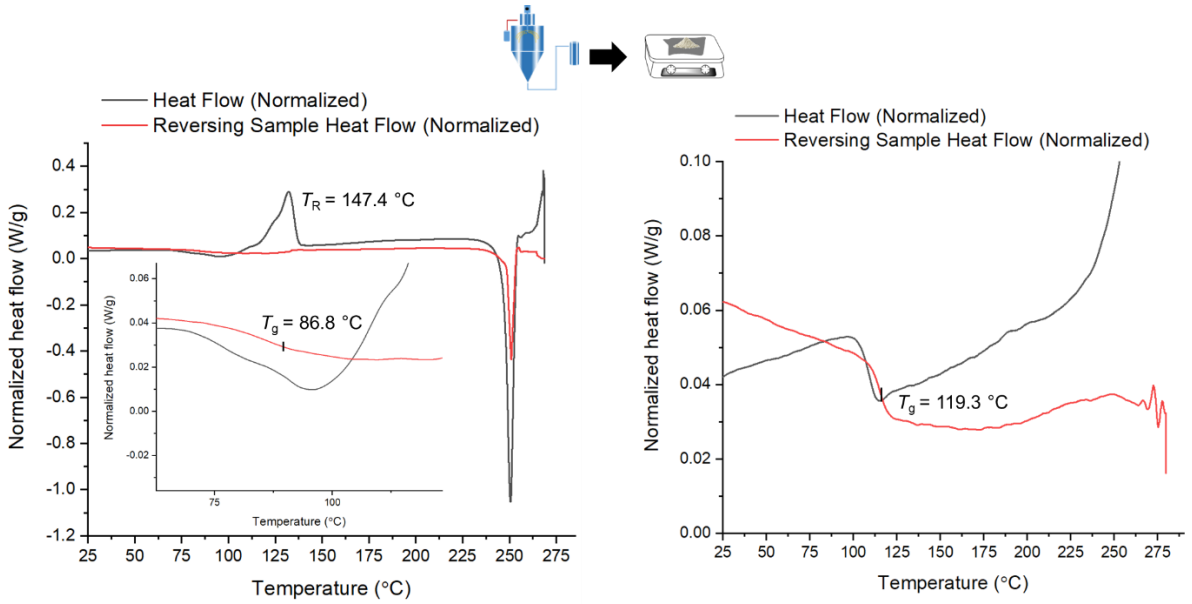

Fig. S36 *m*DSC data of QC of poly*a*morph I obtained by SD.

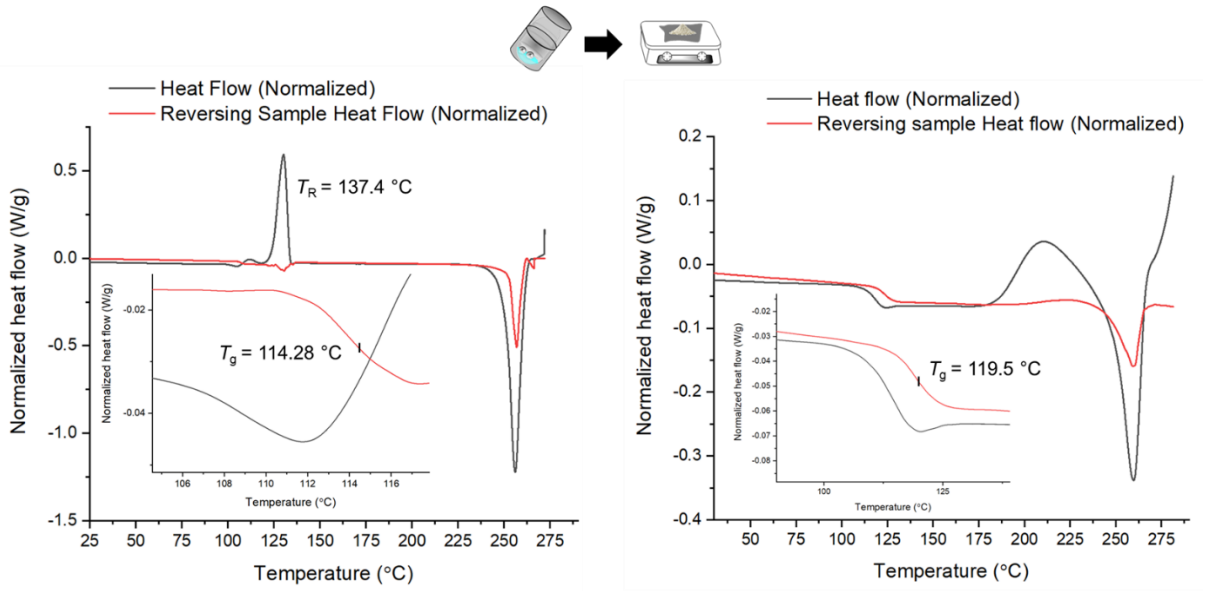

Fig. S37 *m*DSC data of QC of poly*a*morph III obtained by BM.

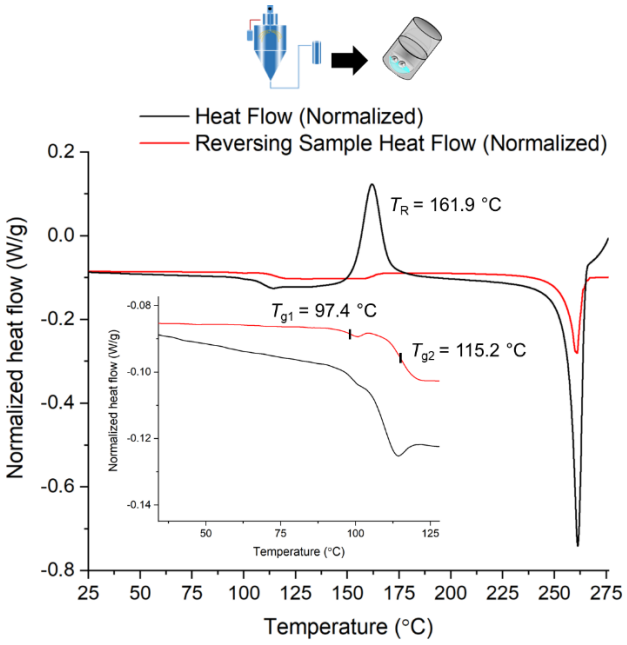

Fig. S38 *m*DSC data of BM of poly*a*morph I obtained by SD.

Total scattering pair distribution function analysis (PDF)

X-ray total scattering data was collected for crystalline and amorphous HCT samples at the beamline P02.1, PETRA III from DESY synchrotron in Hamburg, Germany. All samples were carefully ground and inserted in a 0.7 mm glass capillary that was further sealed. A beam size of 0.2 by 0.2 mm^2 with a fixed high energy of 60 KeV (λ = 0.207 Å) was used. A 2D detector measuring 40 by 40 cm with a sample to detector distance of 375.4 mm was used. A total of 20 diffractograms were collected every 60 seconds with an exposure time of 1 second, giving a total time of 1200 seconds (20 minutes) for each sample. The collected 2D data were further integrated.

The collected X-ray total scattering data was integrated and converted into S(*Q*) and F(*Q*) using PDFgetX3 software.[2] The background scattering signal from the empty glass capillary was further subtracted from the data. A Fourier transformation of the data into PDF was performed using the PDFGetX3 program.[2] The following parameters were used for the data reduction: Q_{min} = 0.6 Å^{-1}, Q_{max} = 16 Å^{-1}, $Q_{maxinst}$ = 16 Å^{-1} and rpoly = 0.9 Å.

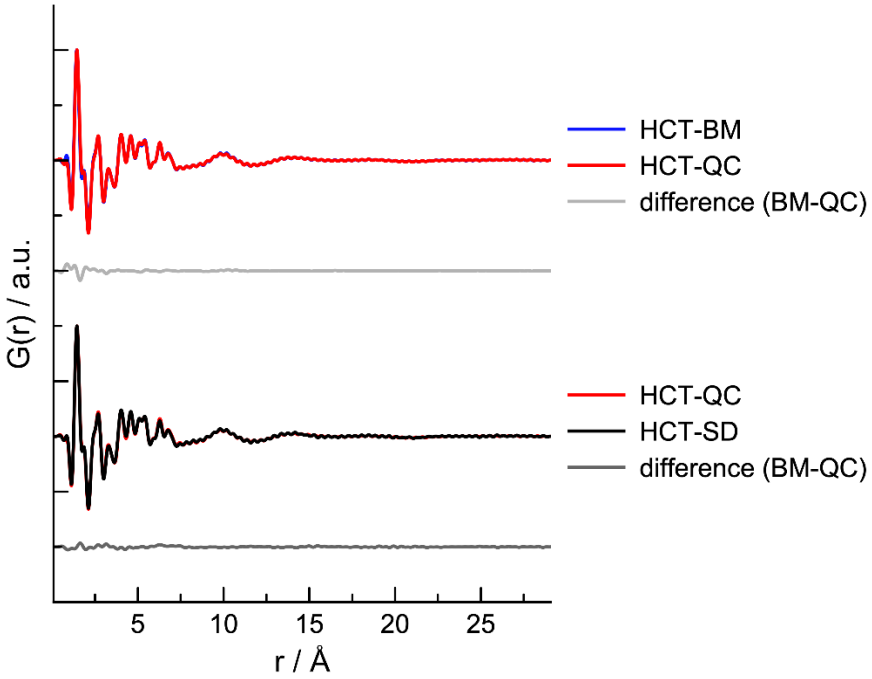

Fig. S39 Experimental PDF data of poly*a*morphs I (HCT-SD), II (HCT-QC) and III (HCT-SD) with the corresponding difference curves.

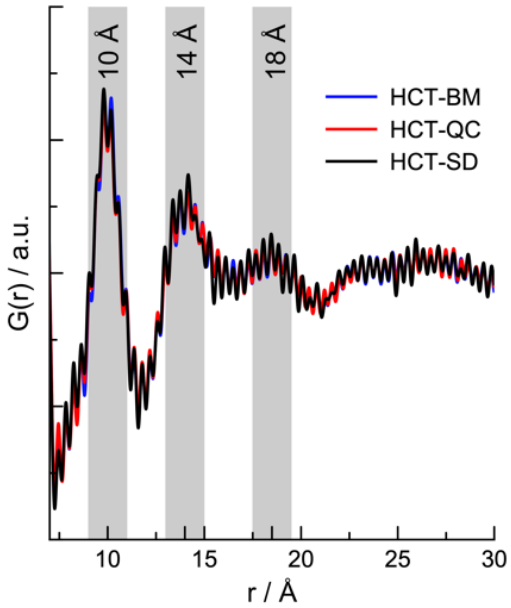

Fig. S40 Zoom-in PDFs on the high *r*-region (7-30 Å) for the three HCT poly*a*morphs.

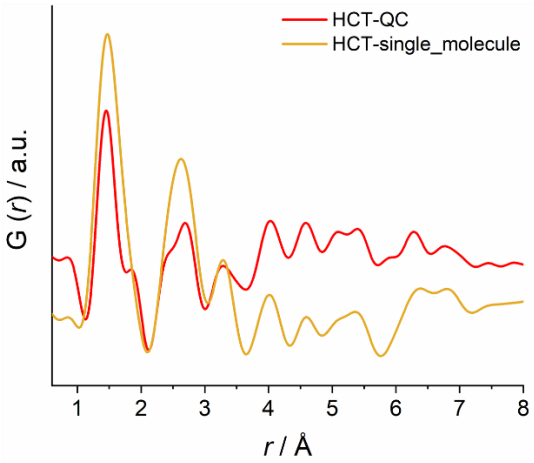

Fig. S41 Experimental and simulated PDFs of poly*a*morph II (HCT-QC) and HCT single molecule.

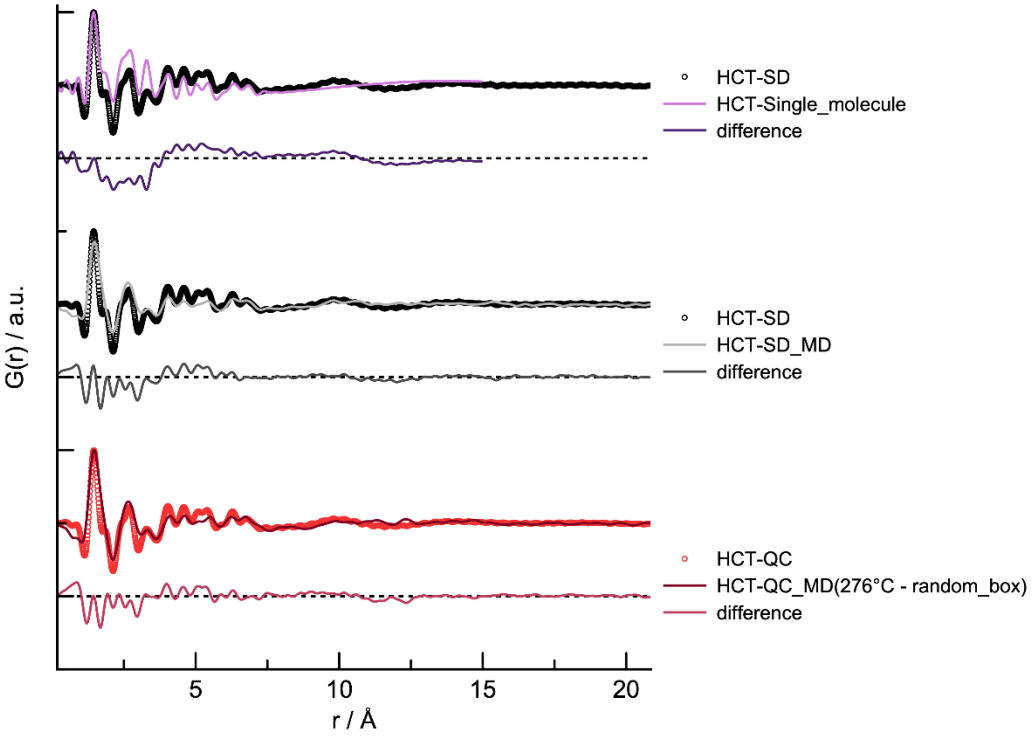

Fig. S42 PDF data of all HCT poly*a*morphs, single molecule and MD models (SD and QC) with the corresponding difference curves.

Molecular dynamics (MD) simulations

Molecular dynamics simulations (MD) of HCT amorphous systems were performed in GROMACS 5.1.1 software package[3] using CHARMM General Force Field (CGenFF).[4, 5] Modelling SD, QC and the melting process requires running MD simulations at very high temperatures compared with what is typically done with force fields. The CHARMM force field family, has been successfully used to study glass transitions and model systems at temperatures of up to 700 K.[6, 7]

For all MD simulations, Lennard-Jones potential to describe dispersion/repulsion forces and the point charge Coulomb potential for electrostatic interactions were used to calculate the intermolecular energy between pairs or neighboring atoms. Long-range electrostatic interactions were accounted for using the particle-mesh Ewald method,[8] with a cutoff of 10 Å for the real space part of the interactions. A cutoff radius of 1.2 nm for the Lennard-Jones potential, and long-range dispersion corrections were added to both energy and pressure. The following specific simulation conditions were used for the preparation of amorphous HCT *via* QC and SD.

MD of SD process: 100 HCT and 1000 ethanol molecules were randomly distributed in a simulation box created by using the '*insert-molecules*' tool from GROMACS.[3] The starting configuration was subjected to energy minimization followed by a 1.0 ns equilibration in isothermal-isobaric NPT ensemble (constant pressure [P], constant particle number [N] and constant temperature [T]). The equilibration state was followed by a production stage, also in the NPT ensemble for additional 20 ns. The time per set was 2 fs. During this period, the temperature was maintained at 80 °C (353.15 K), which was the experimental temperature used for SD. A velocity rescale thermostat was used to control the temperature, while the pressure was kept at 1 bar using a Parrinello-Rahman barostat.[9] Ethanol molecules (5 or 10) were iteratively removed from the box with a segment time (time between removing ethanol molecules) of 10 ps or 100 ps. After each removing of 5 or 10 ethanol molecules, a NPT equilibration with alternated Berendsen and Parrinello-Rahman barostat[9, 10] were used to control the pressure and ensure an anisotropical scale of the box with a coupling time constant of 10 ps. After removing all ethanol molecules, the system was equilibrated under NPT conditions for 2 ns.

MD of QC process: i) *random box approach* – 100 HCT molecules were randomly inserted in a simulation box using the '*insert-molecules*' tool of GROMCAS.[3] An energy minimization followed by NVT simulation (constant volume [V], constant particle number [N] and constant temperature [T]) during 100 ps was performed. A production stage using NPT ensemble for 20 ns at a time per step of 2 fs was used. The simulation temperature started at 25 °C (298.15 K) followed by an increment to 276 °C (550 K, melting temperature of HCT) with a step of 50 °C. At each temperature increment, a NPT simulation was performed for 20 ns. The system was finally equilibrated at 25 °C by running a NPT simulation for another 20 ns. A velocity rescale thermostat was used to control the temperature, while the pressure was kept at 1 bar using Parrinello-Rahman barostat.[9]

ii) *supercell approach* – HCT supercell (10 x 10 x 10) was created using a python script written by Larsen.[11, 12] An initial energy minimization, followed by a NVT simulation of 50 ps and a NPT simulation of 200 ps were performed. The supercell was then heated to 476 °C (750 K) until its melting (*i.e.* until the supercell was 'destroyed' and become an amorphous system) with a temperature step of 50 K. At each temperature increment, a NPT simulation of 10 ns with a time per step of 2 fs was used. For the final temperature of 476 °C, a longer NPT simulation of 40 ns was performed. A Berendsen barostat[10] was used to control the pressure and to scale the supercell anisotropically with a coupling time constant of 10 ps. An equilibration NPT simulation was performed at 25 °C for 10 ns.

Considering that 476 °C (750 K) is a largely overestimated temperature for the melting process, we have performed two additional simulations, with the same MD steps previously described. This time, crystal defects were randomly generated in the supercell by removing 2 molecules at the temperature of 326 °C (600 K) and 5 molecules at the temperature of 276 °C (550 K, the experimental melting temperature of HCT).

The last 10 ns of the simulations were used to calculate the PDF (Fig. 4 d and Fig. S43 and S44), using the DiffPy-CMI program,[13] radial distribution functions (Fig. S45) and angular distributions (Fig. 5 and Fig. S46-S49).

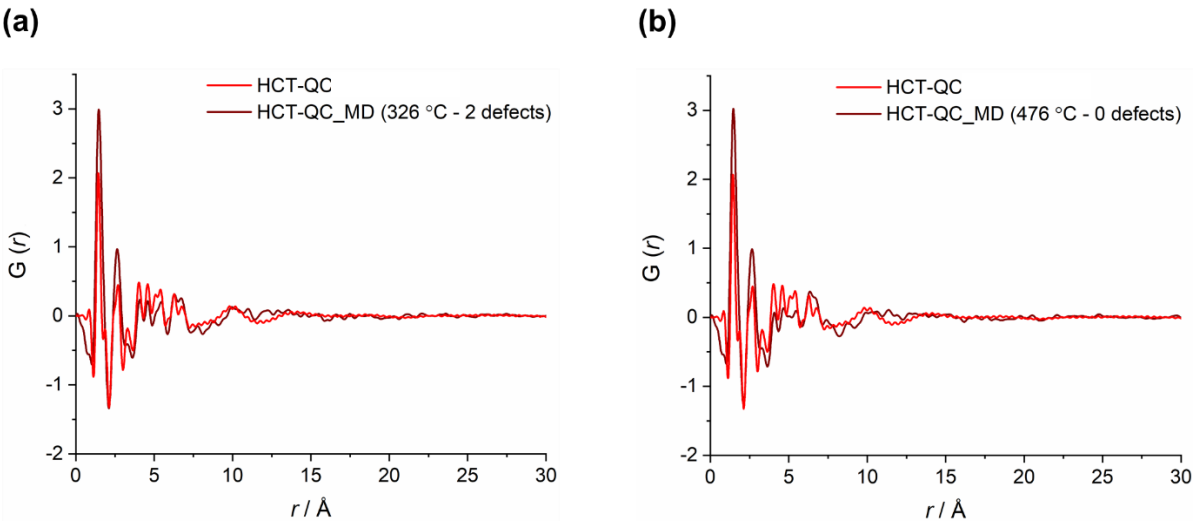

Fig. S43 Experimental PDF of poly*a*morph II (HCT-QC) compared with the simulated PDF obtained from a) QC at 326 °C with 2 defects in the crystal structure and b) QC at 476 °C without defects in the crystal structure.

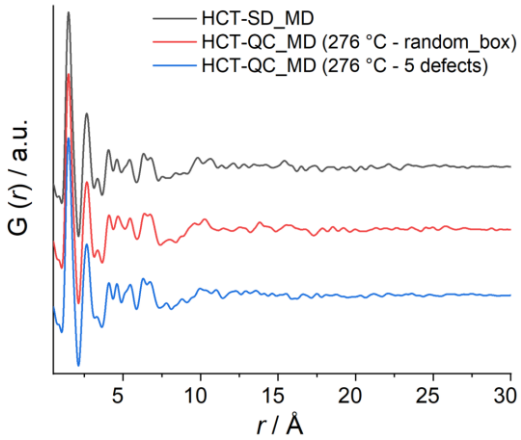

Fig. S44 Simulated PDF (second replica) of poly*a*morph I (HCT-SD) obtained from SD (5 ethanol molecules removed at every 100 ps of simulation), and poly*a*morph II (HCT-QC) obtained from QC at 276 °C using both *random box* and supercell approaches.

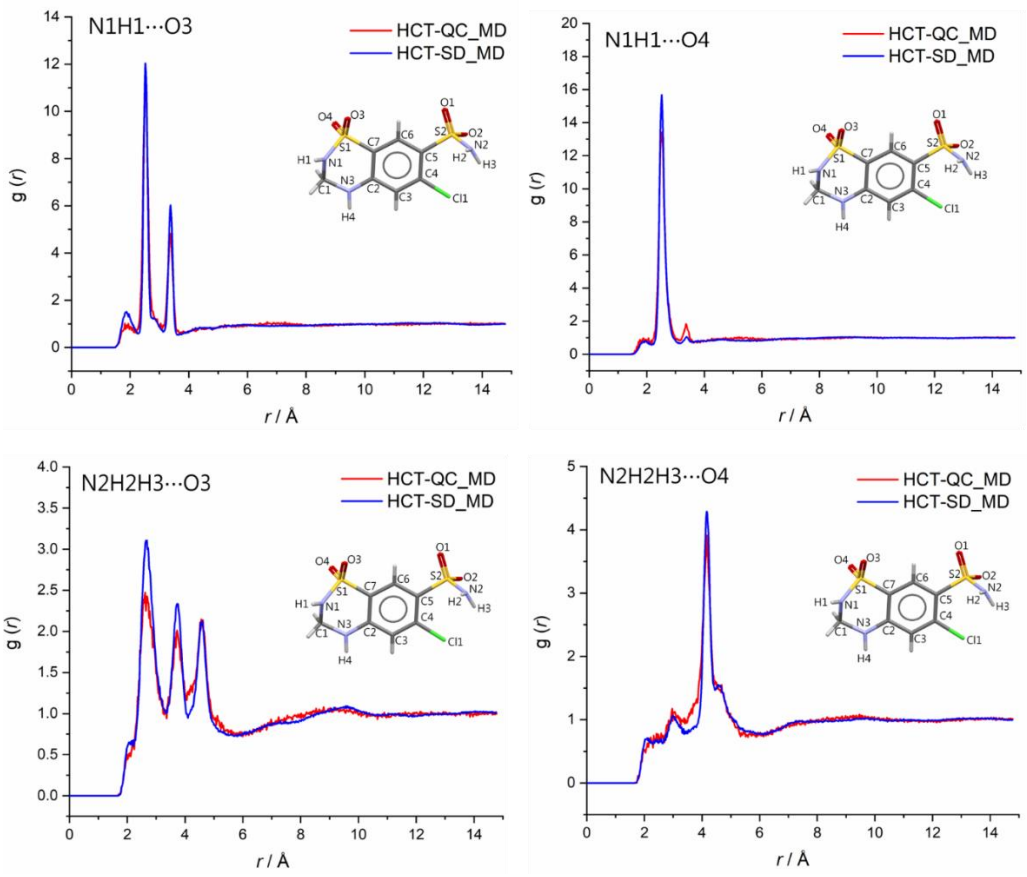

Fig. S45 Radial distribution functions of NH···O interactions present in poly*a*morphs I and II produced by SD and QC.

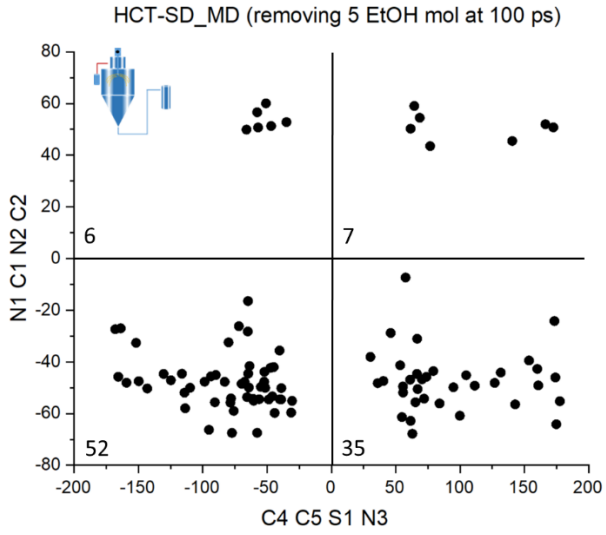

Fig. S46 HCT dihedral angle distributions after SD simulation by removing 5 ethanol (EtOH) molecules at each 100 ps.

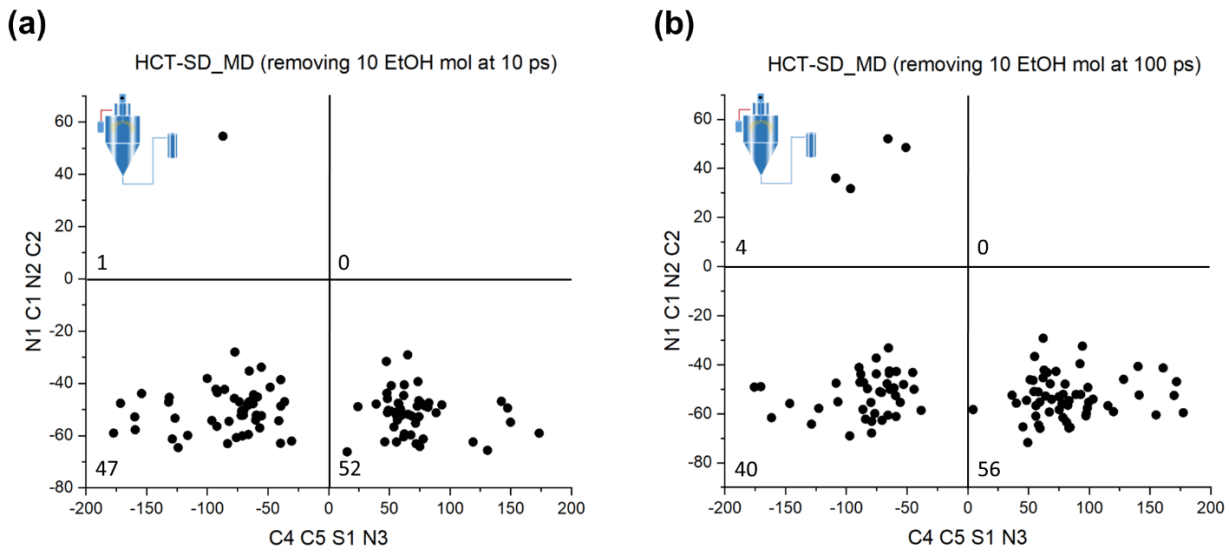

Fig. S47 HCT dihedral angle distributions after SD simulation by removing (a) 10 ethanol (EtOH) molecules at each 10 ps and (b) 10 ethanol (EtOH) molecules at each 100 ps.

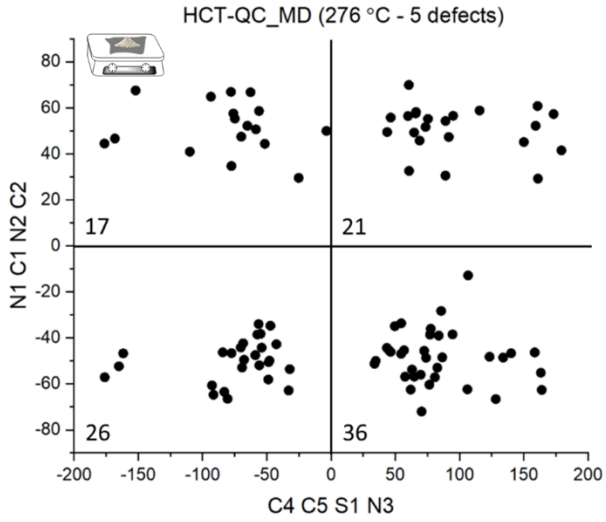

Fig. S48 HCT dihedral angle distributions after MD simulation of QC at 276 °C. 5 defects were introduced in the crystal structure.

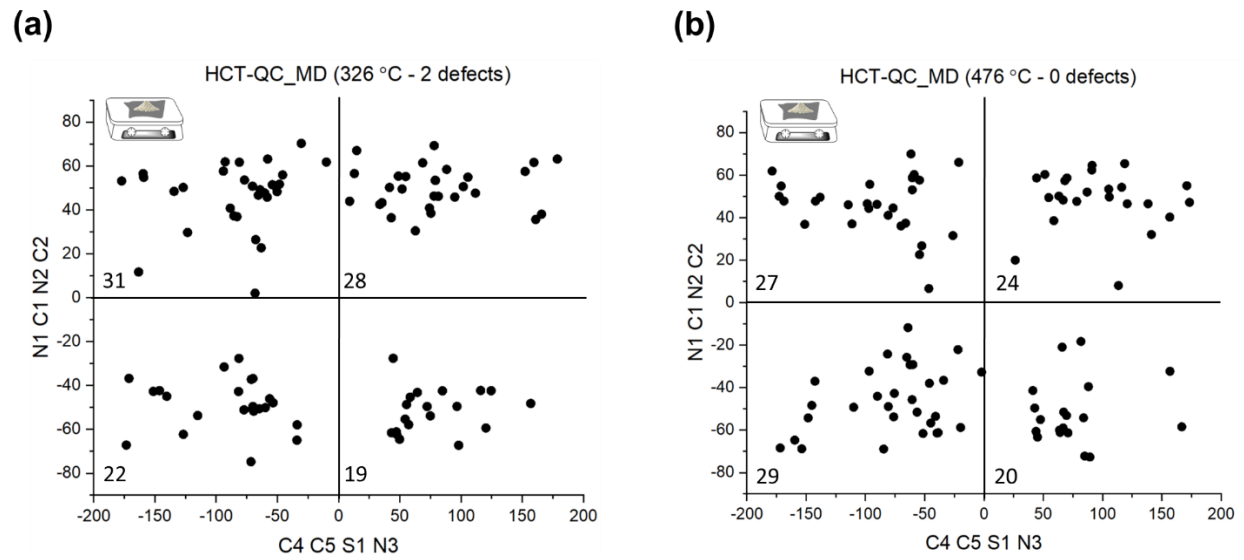

Fig. S49 HCT dihedral angle distributions after MD simulation of QC at 326 °C (a) and 476 °C (b). 2 defects were introduced in the crystal structure for the experiment at 326 °C.

Isothermal microcalorimetry using thermal activity monitor (TAM)

A thermal activity monitor instrument (TA instrument TAM III, New Castle, USA) was used to directly measure the relaxation time of amorphous samples. This equipment collects the rate of enthalpy relaxation as a function of time during annealing.[14] Each sample, around 115 mg, was prepared in 4 mL disposable crimp-sealed ampoules and measured at 25 ℃. In order to reduce the effect of thermal history on sample relaxation, freshly prepared samples were collected and loaded into the equilibrium position. The obtained power-time curves were fitted with the derivative of the "modified stretched exponential'' (MSE) equation to obtain the parameters τ_0, τ_1 and β.[14, 15]

$$P = 277.8\frac{\Delta H_r(\infty)}{\tau_0}(1+\frac{\beta t}{\tau_1})(1+\frac{t}{\tau_1})^{\beta-2}exp\left[-(\frac{t}{\tau_0})(1+\frac{t}{\tau_1})^{\beta-1}\right] \quad (1)$$

Where P is the power (in µW/g) and t the measurement time (in hours). 277.8 is a numerical factor resulting from unit conversions, τ_0 and τ_1 are relaxation time constants, and β reflects the distribution of independently relaxing states ($0 < \beta < 1$). $\Delta H_r(\infty)$ is the enthalpy relaxation at infinite time obtain by equation (2).

$$\Delta H_r(\infty) = (T_g - T) \times \Delta C_P \quad (2)$$

Where T_g is the glass transition temperature, ΔC_P is the heat capacity change at T_g, and T is the temperature of annealing. Relaxation time ($\tau_D{}^{\beta}$) is then calculated from equation (3).

$$\tau_D{}^{\beta} = \left[(\tau_0)^{\frac{1}{\beta}}(\tau_1)^{\frac{(\beta-1)}{\beta}}\right]^{\beta} \quad (3)$$

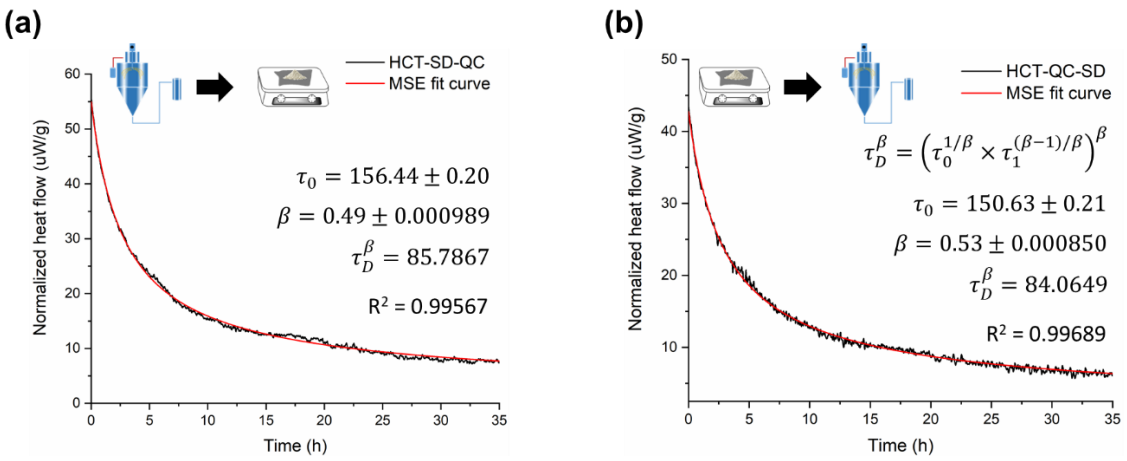

Fig. S50 Relaxation curves and respective τ_D^β values calculated for a) poly*a*morph I obtained by SD and after QC; and b) poly*a*morph II obtained by QC and after SD.

References

1. H. Li, J. He, Q. Liu, Z. Huo, S. Liang, Y. Liang and Y. Ito, *Chromatographia*, 2011, **73**, 171-175.
2. P. Juhas, T. Davis, C. L. Farrow and S. J. L. Billinge, *J. Appl. Crystallogr.*, 2013, **46**, 560-566.
3. M. J. Abraham, T. Murtola, R. Schulz, S. Páll, J. C. Smith, B. Hess and E. Lindahl, *SoftwareX*, 2015, **1-2**, 19-25.
4. K. Vanommeslaeghe, E. Hatcher, C. Acharya, S. Kundu, S. Zhong, J. Shim, E. Darian, O. Guvench, P. Lopes, I. Vorobyov and A. D. Mackerell, Jr., *J. Comput. Chem.*, 2010, **31**, 671-690.
5. R. B. Best, X. Zhu, J. Shim, P. E. M. Lopes, J. Mittal, M. Feig and A. D. MacKerell, Jr., *J. Chem. Theory Comput.*, 2012, **8**, 3257-3273.
6. M. Orselly, J. Devemy, A. Bouvet-Marchand, A. Dequidt, C. Loubat and P. Malfreyt, *ACS Omega*, 2022, **7**, 30040-30050.
7. H. D. Özeren, R. T. Olsson, F. Nilsson and M. S. Hedenqvist, *Materials & Design*, 2020, **187**, 108387.
8. T. Darden, D. York and L. Pedersen, *J. Chem. Phys.*, 1993, **98**, 10089-10092.
9. M. Parrinello and A. Rahman, *J. Appl. Phys.*, 1981, **52**, 7182-7190.
10. H. J. C. Berendsen, J. P. M. Postma, W. F. van Gunsteren, A. DiNola and J. R. Haak, *J. Chem. Phys.*, 1984, **81**, 3684-3690.
11. A. S. Larsen, M. A. Olsen, H. Moustafa, F. H. Larsen, S. P. A. Sauer, J. Rantanen and A. Ø. Madsen, *CrystEngComm*, 2019, **21**, 4020-4024.
12. A. S. Larsen, M. T. Ruggiero, K. E. Johansson, J. A. Zeitler and J. Rantanen, *Cryst. Growth Des.*, 2017, **17**, 5017-5022.
13. P. Juhás, C. L. Farrow, X. Yang, K. R. Knox and S. J. Billinge, *Acta Crystallogr. A Found. Adv.*, 2015, **71**, 562-568.
14. C. Bhugra, R. Shmeis, S. L. Krill and M. J. Pikal, *Pharm. Res.*, 2006, **23**, 2277-2290.
15. J. Liu, D. R. Rigsbee, C. Stotz and M. J. Pikal, *J. Pharm. Sci.*, 2002, **91**, 1853-1862.